Atmospheric Chemistry of $CF_3C(O)OCH_2CF_3$: UV Spectra and Kinetic Data for $CF_3C(O)OCH(\cdot)CF_3$ and $CF_3C(O)OCH(OO\cdot)CF_3$ Radicals, and Atmospheric Fate of $CF_3C(O)OCH(O\cdot)CF_3$ Radicals

T. N. N. Stein, L. K. Christensen, J. Platz, J. Sehested, and O. J. Nielsen*,†

Plant Biology and Biogeochemistry Department, Risø National Laboratory, DK-4000 Roskilde, Denmark

T. J. Wallington*,‡

Ford Research Laboratory, SRL-3083, Ford Motor Company, P.O. Box 2053, Dearborn, Michigan 48121-2053

Received: February 17, 1999; In Final Form: May 17, 1999

Pulse radiolysis transient UV absorption spectroscopy was used to study the ultraviolet absorption spectra (230−330 nm) and kinetics of $CF_3C(O)OCH(\cdot)CF_3$ and $CF_3C(O)OCH(OO\cdot)CF_3$ radicals at 296 K. At 280 nm $\sigma(CF_3C(O)OCH(\cdot)CF_3) = (1.08 \pm 0.13) \times 10^{-18}$ cm^2 molecule^{-1}, at 240 nm $\sigma(CF_3C(O)OCH(OO\cdot)CF_3) = (2.06 \pm 0.24) \times 10^{-18}$ cm^2 molecule^{-1}. Rate constants for the reaction of F atoms with $CF_3C(O)OCH_2CF_3$, the self-reactions of $CF_3C(O)OCH(\cdot)CF_3$ and $CF_3C(O)OCH(OO\cdot)CF_3$ radicals, and the reactions of $CF_3C(O)OCH(OO\cdot)CF_3$ radicals with NO and NO_2 were $(1.8 \pm 0.2) \times 10^{-12}$, $(1.5 \pm 0.2) \times 10^{-11}$, $(7.6 \pm 0.9) \times 10^{-12}$, $(1.5 \pm 0.2) \times 10^{-11}$, and $(8.5 \pm 0.9) \times 10^{-12}$ cm^3 molecule^{-1} s^{-1}, respectively. The atmospheric fate of $CF_3C(O)OCH(O\cdot)CF_3$ radicals was investigated in a FTIR smog chamber. Three loss processes for the $CF_3C(O)OCH(O\cdot)CF_3$ radicals were identified at 296 K and 700 Torr total pressure, reaction with O_2 to form $CF_3C(O)OC(O)CF_3$, α-rearrangement to form $CF_3C(O)\cdot$ radicals and $CF_3C(O)OH$, and decomposition via a mechanism which is unclear. In 760 Torr of air at 296 K, 65% of the $CF_3C(O)OCH(O\cdot)CF_3$ radicals react with oxygen, 18% undergo α-rearrangement, while the fate of the remaining 17% is unclear.

1. Introduction

Recognition of the adverse effect of chlorofluorocarbon (CFC) release into the atmosphere[1,2] has led to an international effort to replace CFCs with environmentally acceptable alternatives. Hydrofluoroethers (HFEs) are fluids designed to replace CFCs in applications such as the cleaning of electronic equipment, heat transfer agents in refrigeration systems, and carrier fluids for lubricant deposition.[3] HFEs are volatile compounds and will be released into the atmosphere during its use. In the atmosphere, photochemical oxidation of HFEs will lead to the formation of fluorinated esters and fluorinated formates.[4−7] The atmospheric fate of these products is unknown at the present. To improve our understanding of the atmospheric chemistry of esters we have studied the atmospheric chemistry of 2,2,2-trifluoroethyl trifluoroacetate $CF_3C(O)OCH_2CF_3$ (bp = 55.0 °C.). This compound provides insight into the behavior of alkyl, alkyl peroxy, and alkoxy radicals formed α to the ester functionality.

The atmospheric oxidation of $CF_3C(O)OCH_2CF_3$ will be initiated by reaction with OH radicals. The radical formed, $CF_3C(O)OCH(\cdot)CF_3$, will add O_2 rapidly to give a $CF_3C(O)OCH(OO\cdot)CF_3$ radical.

$$CF_3C(O)OCH_2CF_3 + OH \rightarrow CF_3C(O)OCH(\cdot)CF_3 + H_2O \quad (1)$$

$$CF_3C(O)OCH(\cdot)CF_3 + O_2 + M \rightarrow CF_3C(O)OCH(OO\cdot)CF_3 \quad (2)$$

By analogy to other peroxy radicals,[8,9] $CF_3C(O)OCH(OO\cdot)CF_3$ radicals will react with NO, NO_2, HO_2, and other peroxy radicals in the atmosphere.

$$CF_3C(O)OCH(OO\cdot)CF_3 + NO \rightarrow CF_3C(O)OCH(O\cdot)CF_3 + NO_2 \quad (3a)$$

$$CF_3C(O)OCH(OO\cdot)CF_3 + NO + M \rightarrow CF_3C(O)OCH(ONO_2)CF_3 + M \quad (3b)$$

$$CF_3C(O)OCH(OO\cdot)CF_3 + NO_2 + M \rightarrow CF_3C(O)OCH(OONO_2)CF_3 + M \quad (4)$$

$$CF_3C(O)OCH(OO\cdot)CF_3 + HO_2 \rightarrow \text{products} \quad (5)$$

$$CF_3C(O)OCH(OO\cdot)CF_3 + R'O_2 \rightarrow \text{products} \quad (6)$$

A pulse radiolysis time-resolved UV−visible absorption spectroscopic technique was used to measure the UV absorption spectra of $CF_3C(O)OCH(\cdot)CF_3$ and $CF_3C(O)OCH(OO\cdot)CF_3$ radicals, and to study the kinetics of reactions 3, 4, and 6. In the case of reaction 6 we studied the self-reaction of the peroxy radical ($R'O_2 = CF_3C(O)OCH(OO\cdot)CF_3$). A smog chamber FTIR method was used to study the atmospheric fate of $CF_3C(O)OCH(O\cdot)CF_3$ radicals.

2. Experimental Section

The two experimental systems used are described in detail elsewhere.[10,11] Unless stated otherwise, all quoted errors are two

* Author to whom correspondence should be addressed.
† E-mail: ole.john.nielsen@risoe.dk.
‡ E-mail: twalling@ford.com.

10.1021/jp990599t CCC: $18.00
Published on Web 06/30/1999

standard deviations from least-squares analysis of the data.

2.1. Pulse Radiolysis System at Risø National Laboratory. A pulse radiolysis transient UV absorption apparatus[10] was used to study the UV absorption spectra and kinetics of $CF_3C(O)OCH(\cdot)CF_3$ and $CF_3C(O)OCH(OO\cdot)CF_3$ radicals. Radicals were generated by radiolysis of gas mixtures in a 1 L stainless steel reactor by a 30 ns pulse of 2 MeV electrons from a Febetron 705B field emission accelerator. The radiolysis dose, referred to herein as a fraction of the maximum dose, was varied by insertion of stainless steel attenuators between the accelerator and the chemical reactor. The analysis light was provided by a pulsed Xenon arc lamp, reflected in the reaction cell by internal white type optics, dispersed using a 1 m McPherson Monochromator (operated at a spectral resolution of 0.8 nm), and detected by a photomultiplier. All transients were results of single-pulse experiments with no signal averaging.

SF_6 was used as the diluent gas. Radiolysis of SF_6 produces fluorine atoms.

$$SF_6 \xrightarrow{2\ \mathrm{MeV}e^-} F + \text{products} \qquad (7)$$

SF_6 was always present in great excess to minimize the relative importance of direct radiolysis of other compounds in the gas mixtures. The fluorine atom yield was determined by measuring the yield of CH_3O_2 radicals following radiolysis of mixtures of 10 mbar of CH_4, 40 mbar of O_2, and 950 mbar of SF_6:

$$F + CH_4 \rightarrow CH_3 + HF \qquad (8)$$

$$CH_3 + O_2 + M \rightarrow CH_3O_2 + M \qquad (9)$$

CH_3O_2 radicals were monitored using their absorption at 260 nm. Based upon $\sigma_{260\ nm}(CH_3O_2) = 3.18 \times 10^{-18}$ cm^2 molecule^{-1},[8] the F atom yield at full radiolysis dose and 1000 mbar SF_6 was determined to be $(2.98 \pm 0.33) \times 10^{15}$ cm^{-3}. The quoted uncertainty reflects both statistical uncertainties associated with the calibration procedure and a 10% uncertainty in $\sigma_{260\ nm}(CH_3O_2)$.[8]

Reagents used were 2−30 mbar of $CF_3C(O)OCH_2CF_3$, 0−50 mbar O_2 (ultrahigh purity), 0−0.81 mbar of NO (>99.8%), and 0−0.70 mbar of NO_2 (>98%). The $CF_3C(O)OCH_2CF_3$ sample (>97%) was repeatedly degassed by freeze−pump−thaw cycles before use. Three sets of experiments were performed using the pulse radiolysis system. First, the radiolysis of SF_6/$CF_3C(O)OCH_2CF_3$ mixtures was used to study the kinetics of the reaction of F atoms with $CF_3C(O)OCH_2CF_3$ and the UV spectrum and kinetics of the $CF_3C(O)OCH(\cdot)CF_3$ alkyl radical. Second, the radiolysis of $SF_6/CF_3C(O)OCH_2CF_3/O_2$ mixtures was used to study the UV spectrum and kinetics of the $CF_3C(O)OCH(OO\cdot)CF_3$ alkyl peroxy radical. Third, the radiolysis of $SF_6/CF_3C(O)OCH_2CF_3/NO_X$ mixtures was used to study the rates of reactions of the $CF_3C(O)OCH(OO\cdot)CF_3$ radical with NO and NO_2.

A Princeton Applied Research OMA-II diode array was used to measure the UV absorption spectra of the $CF_3C(O)OCH(\cdot)CF_3$ and $CF_3C(O)OCH(OO\cdot)CF_3$ radicals. The diode array was installed at the exit slit of the monochromator in place of the photomultiplier, which was used for measuring transient absorptions. The setup consisted of the diode array, an image amplifier (type 1420−1024HQ), a controller (type 1421), and a personal computer used for data acquisition, handling, and storage. Spectral calibrations were achieved using a Hg pen ray lamp.

2.2. FTIR Smog Chamber System at Ford Motor Company. All experiments were performed in a 140 L Pyrex reactor interfaced to a Mattson Sirus 100 FTIR spectrometer.[11] The reactor was surrounded by 22 fluorescent blacklamps (GE F15T8-BL) which were used to photochemically initiate the experiments. The oxidation of $CF_3C(O)OCH_2CF_3$ was initiated by reaction with Cl atoms generated by the photolysis of molecular chlorine in O_2/N_2 diluent at 700 Torr (760 Torr = 1013 mbar) total pressure at 295 ± 2 K:

$$Cl_2 + h\nu \rightarrow 2\ Cl \qquad (10)$$

$$Cl + CF_3C(O)OCH_2CF_3 \rightarrow CF_3C(O)OCH(\cdot)CF_3 + HCl \qquad (11)$$

$$CF_3C(O)OCH(\cdot)CF_3 + O_2 + M \rightarrow CF_3C(O)OCH(OO\cdot)CF_3 + M \qquad (2)$$

Loss of $CF_3C(O)OCH_2CF_3$ and formation of products were monitored by FTIR spectroscopy using an infrared path length of 28 m and a resolution of 0.25 cm^{-1}. Infrared spectra were derived from 32 co-added interferograms.

The products of the atmospheric oxidation of $CF_3C(O)OCH_2CF_3$ were investigated by irradiating $CF_3C(O)OCH_2CF_3/Cl_2/O_2/N_2$ mixtures at a total pressure of 700 Torr. Initial concentrations of the gas mixtures were 3−5 mTorr of $CF_3C(O)OCH_2CF_3$, 0.1−2 Torr of Cl_2, and 5−700 Torr of O_2 in N_2 diluent. Reference spectra of $CF_3C(O)OC(O)CF_3$ and $CF_3C(O)OH$ were generated by expanding known volumes of these compound into the chamber.

In smog chamber experiments unwanted loss of reactants and products via photolysis, dark chemistry, and wall reactions have to be considered. Control experiments were performed to check for such unwanted losses in the chamber; none was observed. No significant loss of $CF_3C(O)OCH_2CF_3$ (<2%), $CF_3C(O)OC(O)CF_3$ (<2%), or $CF_3C(O)OH$ (<4%) was observed when mixtures of these compounds in air diluent were irradiated, showing that photolysis of $CF_3C(O)OCH_2CF_3$, $CF_3C(O)OH$, and $CF_3C(O)OC(O)CF_3$ in the chamber is not important. When reaction mixtures containing $CF_3C(O)OC(O)CF_3$ and Cl_2 were irradiated in the chamber no loss of $CF_3C(O)OC(O)CF_3$ was observed, showing there are no reactions between $CF_3C(O)OC(O)CF_3$ and Cl and/or Cl_2.

3. Results

3.1. Kinetics of the F + $CF_3C(O)OCH_2CF_3$ Reaction. Following the pulse radiolysis of $CF_3C(O)OCH_2CF_3/SF_6$ mixtures, a rapid increase in absorption in the UV at 280 nm followed by a slower decay was observed. We ascribe the increase in absorption to formation of $CF_3C(O)OCH(\cdot)CF_3$ radicals via reaction 12:

$$F + CF_3C(O)OCH_2CF_3 \rightarrow CF_3C(O)OCH(\cdot)CF_3 + HF \qquad (12)$$

Experiments were conducted using 2.70−6.36 mbar of $CF_3C(O)OCH_2CF_3$ and 1000 mbar of SF_6 at 9.4% of full radiolysis dose; in all experiments the formation of $CF_3C(O)OCH(\cdot)CF_3$ radicals followed pseudo-first-order kinetics. Pseudo-first-order rate constants (k^{first}) were derived from a fit of a first-order rise expression to the transient absorptions, where $A(t)$ is the time-dependent absorbance, A_0 is the extrapolated absorbance at $t = 0$ (always close to zero), and A_{inf} is the absorbance at infinite time. The insert in Figure 1 shows a typical transient

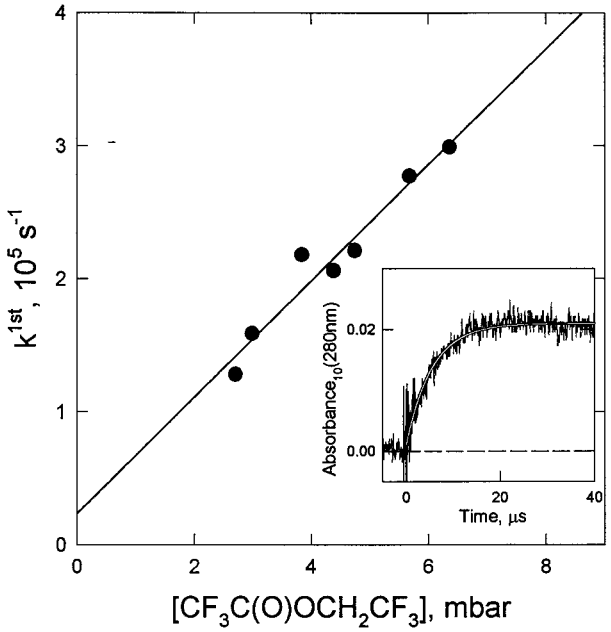

Figure 1. Pseudo-first-order formation rate constant of $CF_3C(O)OCH(\cdot)CF_3$ radicals versus the initial $CF_3C(O)OCH_2CF_3$ concentration. The insert shows a typical transient absorption with an initial $CF_3C(O)OCH_2CF_3$ concentration of 2.99 mbar and a radiolysis dose of 9.4%, the smooth line is the first-order fit giving $k^{first} = 1.6 \times 10^5$ s^{-1}.

absorption (with an initial $CF_3C(O)OCH_2CF_3$ concentration of 2.99 mbar), the smooth line is the first-order fit giving $k^{first} = 1.6 \times 10^5$ s^{-1}. Figure 1 shows the measured pseudo-first-order formation rate constants versus the concentration of $CF_3C(O)OCH_2CF_3$. A linear least-squares analysis gives $k_{12} = (1.78 \pm 0.23) \times 10^{-12}$ cm^3 $molecule^{-1}$ s^{-1}.

3.2. UV Absorption Spectrum of the $CF_3C(O)OCH(\cdot)CF_3$ Radical. Following the pulse radiolysis of mixtures of 3 mbar of $CF_3C(O)OCH_2CF_3$ and 997 of mbar SF_6, a rapid (complete within 5−8 μs) increase in absorption at 280 nm was observed, followed by a slower decay. Since no absorption was observed when only $CF_3C(O)OCH_2CF_3$ or SF_6 was subject to pulse radiolysis, we ascribe the absorption in Figure 2A to formation of $CF_3C(O)OCH(\cdot)CF_3$ radicals via reaction 12 and their subsequent loss via self-reaction 13:

$$CF_3C(O)OCH(\cdot)CF_3 + CF_3C(O)OCH(\cdot)CF_3 + M \rightarrow \text{products} \quad (13)$$

We assume that F atoms react with $CF_3C(O)OCH_2CF_3$ exclusively via H-atom abstraction. To determine the absorption cross section of the $CF_3C(O)OCH(\cdot)CF_3$ radical at 280 nm, the maximum transient absorbance was recorded at various radiolysis doses (and hence various initial radical concentrations). Figure 3A shows a plot of the maximum transient absorption, A_{max}, versus radiolysis dose. Using an initial $CF_3C(O)OCH_2CF_3$ concentration of 3 mbar the absorbance increases linearly up to 22% of full dose, suggesting that unwanted radical−radical reactions, such as reactions 13 and 14, are unimportant for low radiolysis doses:

$$F + CF_3C(O)OCH(\cdot)CF_3 \rightarrow \text{products} \quad (14)$$

Linear least-squares regression of the low-dose data in Figure 3A gives a slope of 0.223 ± 0.009. Combining this result with the calibrated fluorine atom yield of $(2.98 \pm 0.33) \times 10^{15}$ cm^{-3} (at full dose and 1000 mbar of SF_6) and the optical path length

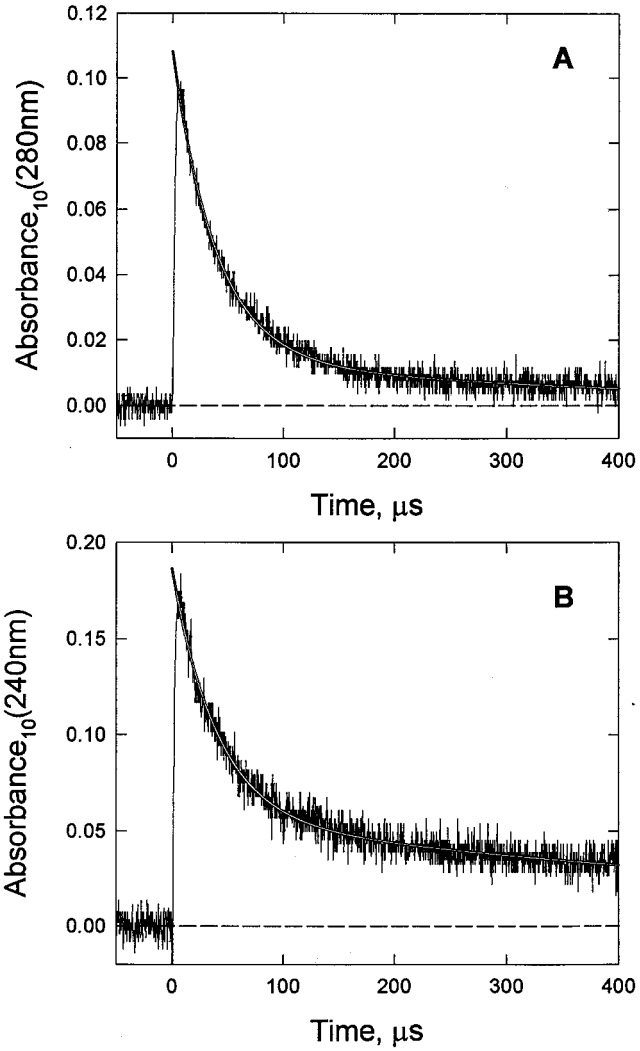

Figure 2. Transient absorption following radiolysis of mixtures of (A) 10 mbar of $CF_3C(O)OCH_2CF_3$ and 990 mbar of SF_6 (0.42 dose) at 280 nm, and (B) 15 mbar of $CF_3C(O)OCH_2CF_3$, 15 mbar of O_2, and 970 mbar of SF_6 (full dose) at 240 nm. The UV analysis path lengths were 160 and 80 cm, respectively. Absorption is ascribed to (A) $CF_3C(O)OCH(\cdot)CF_3$ radicals and (B) $CF_3C(O)OCH(OO\cdot)CF_3$ radicals. The smooth lines are second-order decay fits.

of 160 cm gives $\sigma_{280\ nm}(CF_3C(O)OCH(\cdot)CF_3) = (1.08 \pm 0.13) \times 10^{-18}$ cm^2 $molecule^{-1}$. The UV absorption spectrum was measured by combining three diode array spectra (7.5 μs delay, 3 μs integration time, and 1 nm resolution) in the range 230−330 nm. The observed spectrum was placed on an absolute basis using $\sigma_{280\ nm} = 1.08 \times 10^{-18}$ cm^2 $molecule^{-1}$, the result is shown in Figure 4A.

3.3. Kinetics of the Self-Reaction of the $CF_3C(O)OCH(\cdot)CF_3$ Radical. The rate constant for self-reaction of $CF_3C(O)OCH(\cdot)CF_3$ radicals was determined by monitoring the rate of decay of the absorption at 280 nm following pulse radiolysis of mixtures of 10 mbar of $CF_3C(O)OCH_2CF_3$ and 990 mbar of SF_6. Half-lives of the decays were derived from fits to the experimental transients using a second-order expression: $A(t) = A_{inf} + (A_0 - A_{inf})/(1 + k'(A_0 - A_{inf})t)$, where $A(t)$ is the time-dependent absorbance, A_{inf} is the absorbance at $t = \infty$ (always close to zero), A_0 is the fitted absorbance at $t = 0$, and $k' = 2k_{13}\ln 10/(l\sigma_{280\ nm}(CF_3C(O)OCH(\cdot)CF_3))$, k_{13} is the rate constant for reaction 13, and l is the optical path length (160 cm). The decays were always well-described by the second-order expression above. An example of a fit is shown in Figure 2A. Figure 5A shows the reciprocal of the decay half-lives at various doses

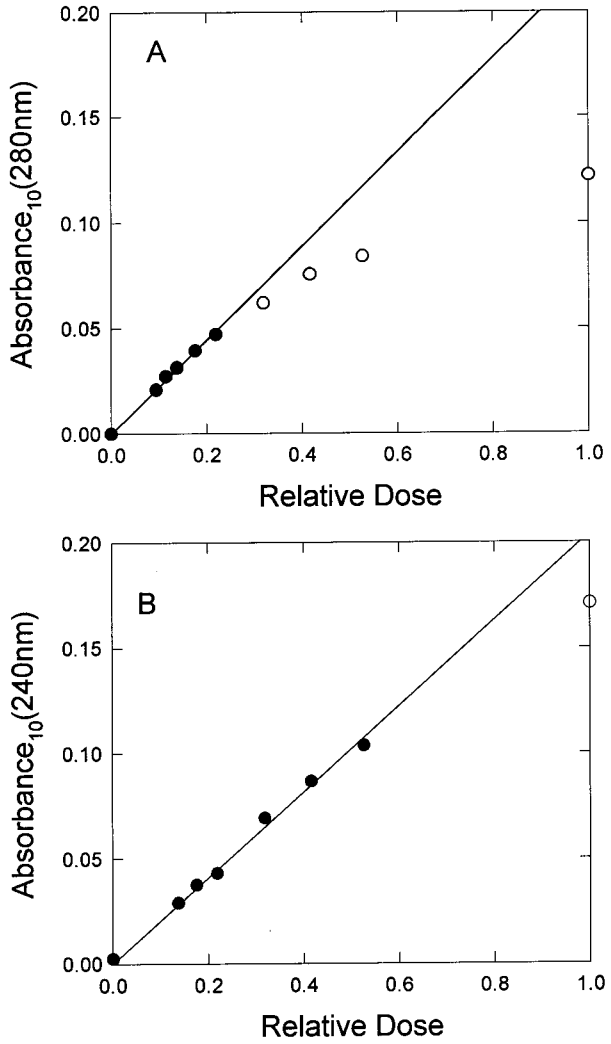

Figure 3. Maximum transient absorptions observed following radiolysis of mixtures of (A) 3 mbar of $CF_3C(O)OCH_2CF_3$ and 997 mbar of SF_6 (UV path length 160 cm), and (B) 15 mbar of $CF_3C(O)OCH_2CF_3$, 15 mbar of O_2, and 970 mbar of SF_6 (UV path length 80 cm). Solid lines are linear least-squares fits to the low dose data (filled circles).

versus A_0. A linear least-squares regression to the experimental data gives a slope of $(3.96 \pm 0.16) \times 10^5\ s^{-1} = (k_{13} \times 2\ \ln 10)/(\sigma_{280\ nm}(CF_3C(O)OCH(\cdot)CF_3) \times l)$. Using $\sigma_{280\ nm}(CF_3C(O)OCH(\cdot)CF_3) = (1.08 \pm 0.13) \times 10^{-18}$ cm^2 molecule^{-1}, we derive $k_{13} = (1.49 \pm 0.19) \times 10^{-11}$ cm^3 molecule^{-1} s^{-1}. The quoted uncertainty includes uncertainties in both the linear least-squares regression shown in Figure 5A and in $\sigma_{280\ nm}(CF_3C(O)OCH(\cdot)CF_3)$.

3.4. UV Absorption Spectrum of the $CF_3C(O)OCH(OO\cdot)CF_3$ Radical. To study the UV spectrum of the peroxy radical $CF_3C(O)OCH(OO\cdot)CF_3$, mixtures of 15 mbar of $CF_3C(O)OCH_2CF_3$, 15 mbar of O_2, and 970 mbar of SF_6 were subjected to pulse radiolysis and the resulting transient absorbance was monitored at 240 nm. A typical experimental absorption transient is shown in Figure 2B. We attribute the absorption observed using $SF_6/CF_3C(O)OCH_2CF_3/O_2$ mixtures to the formation of $CF_3C(O)OCH(OO\cdot)CF_3$ radicals by reactions 12 and 2.

To derive the UV absorption spectrum of the $CF_3C(O)OCH(OO\cdot)CF_3$ radical we need to work under conditions where unwanted secondary radical−radical reactions such as reactions 13−17 are avoided or minimized.

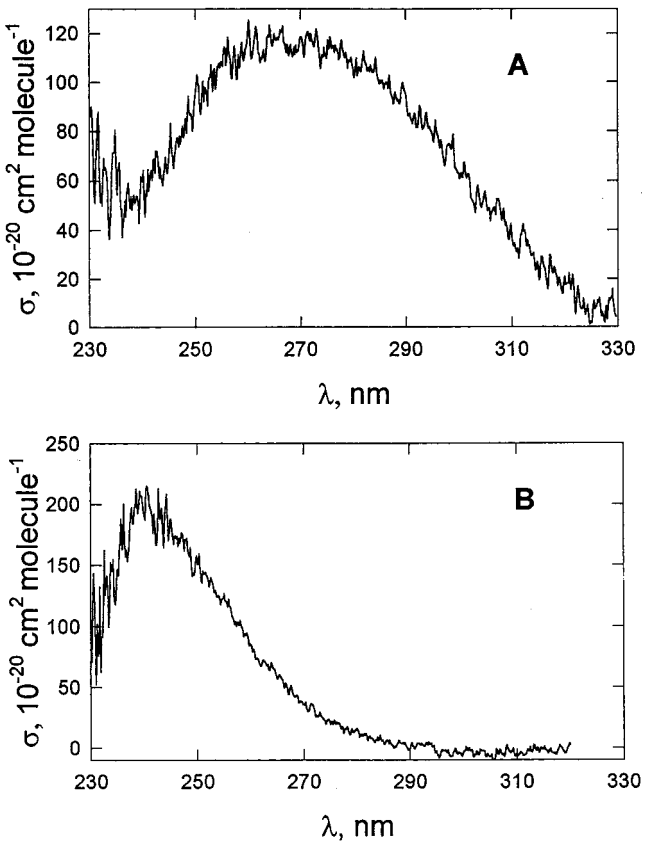

Figure 4. Absorption spectrum of (A) $CF_3C(O)OCH(\cdot)CF_3$ and (B) $CF_3C(O)OCH(OO\cdot)CF_3$.

$$CF_3C(O)OCH(OO\cdot)CF_3 + CF_3C(O)OCH(OO\cdot)CF_3 \rightarrow \text{products} \quad (15)$$

$$CF_3C(O)OCH(OO\cdot)CF_3 + CF_3C(O)OCH(\cdot)CF_3 \rightarrow \text{products} \quad (16)$$

$$CF_3C(O)OCH(OO\cdot)CF_3 + F \rightarrow \text{products} \quad (17)$$

In addition, the reaction of F atoms with O_2 needs to be minimized:

$$F + O_2 + M \rightarrow FO_2 + M \quad (18)$$

To minimize the amount of F atoms consumed by reaction 18, the oxygen concentration should be low. However, a low oxygen concentration will increase the importance of reactions 13, 14, and 16. Clearly, a compromise is needed. An initial O_2 concentration of 15 mbar was chosen. Under these experimental conditions 9.7% of the F atoms are converted into FO_2 ($k_{18} = 1.9 \times 10^{-13}$ [12] and $k_{12} = 1.78 \times 10^{-12}$ cm^3 molecule^{-1} s^{-1}).

There are no literature data concerning the kinetics of reactions 14, 16, 17, so we cannot calculate their importance. To check for these unwanted radical−radical reactions the transient absorption at 240 nm was measured in experiments using 15 mbar of $CF_3C(O)OCH_2CF_3$, 15 mbar of O_2, and 970 mbar of SF_6 with the radiolysis dose (and hence initial radical concentration) varied over an order of magnitude. The UV path length was 80 cm. Figure 3B shows a plot of the maximum absorbance versus radiolysis dose. As seen from Figure 3B, the absorption is linear with radiolysis dose up to 53% of maximum dose. This linearity indicates that at low radiolysis doses unwanted secondary radical−radical reactions are not important. The line drawn through the data in Figure 3B is a linear least-

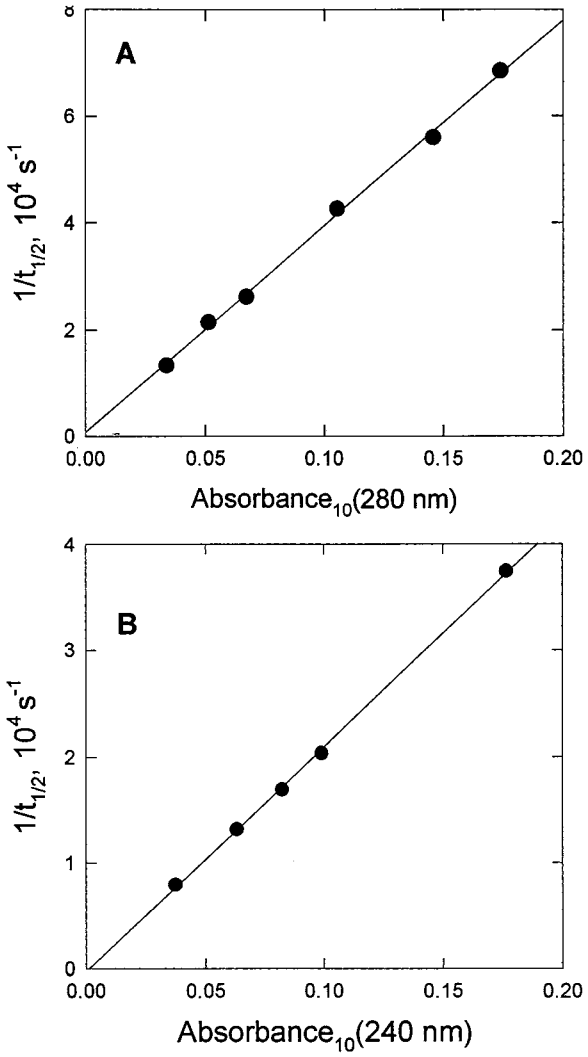

Figure 5. Reciprocal half-lives for the self-reactions of (A) $CF_3C(O)OCH(\cdot)CF_3$ versus A_0 (fitted absorbance at $t = 0$) at 280 nm, and (B) $CF_3C(O)OCH(OO\cdot)CF_3$ versus A_0 (fitted absorbance at $t = 0$) at 240 nm.

squares fit to the low dose data, which gives a slope of 0.204 ± 0.007. From this and three additional pieces of information—(i) the F atom yield of (2.98 ± 0.33) × 10^{15} cm^{-3} (full dose and 1000 mbar of SF_6), (ii) the conversion of F atoms into $CF_3C(O)OCH(OO\cdot)CF_3$ (90.3%) and FO_2 (9.7%), and (iii) the absorption cross section for FO_2 ($\sigma_{240\ nm}$ = 1.80 × 10^{-18} cm^2 $molecule^{-1}$ [12]), we derive $\sigma_{240\ nm}(CF_3C(O)OCH(OO\cdot)CF_3)$ = (2.06 ± 0.24) × 10^{-18} cm^2 $molecule^{-1}$. The quoted uncertainty reflects two standard deviations from a linear least-squares fit to the low dose data in Figure 3B and uncertainty in the absolute calibration of the F atom yield.

The UV absorption spectrum of the $CF_3C(O)OCH(OO\cdot)CF_3$ radical over the range 230−320 nm was measured using the diode array with a 7.5 μs delay, 3 μs integration time, and 1 nm resolution. Using literature data for the UV spectrum of FO_2 radicals,[13] corrections for the presence of FO_2 radicals were applied $\sigma_{corrected} = (\sigma_{raw} - \sigma_{FO_2} \times 0.097)/0.903$. The measured UV spectrum shown in Figure 4B was scaled to the absorption cross section at 240 nm obtained from Figure 3B. The UV spectra of alkyl peroxy radicals typically consist of a single broad, structureless feature in the region 200−300 nm with a width of 40−50 nm and a maximum cross section located at 235−245 nm of (4−5) × 10^{-18} cm^2 $molecule^{-1}$.[8,9] Fluorine substitution results in a blue shift of 10−20 nm.[8,9] The spectrum for the $CF_3C(O)OCH(OO\cdot)CF_3$ radical shown in Figure 4B is broadly consistent with that expected on the basis of the published spectra of other peroxy radicals.[8,9]

3.5. Kinetics of the Self-Reaction of $CF_3(C(O)OCH(OO\cdot)CF_3$ Radicals. Figure 2B shows a typical transient absorption observed following the pulsed radiolysis of $CF_3C(O)OCH_2CF_3/SF_6/O_2$ mixtures. The decay of the absorption is due to the self-reaction of the $CF_3C(O)OCH(OO\cdot)CF_3$ radical:

$$CF_3C(O)OCH(OO\cdot)CF_3 + CF_3C(O)OCH(OO\cdot)CF_3 \rightarrow \text{products} \quad (15)$$

The rate constant of reaction 15 is defined by the equation $-d[RO_2]/dt = 2k_{15obs}[RO_2]^2$. The observed rate constant k_{15obs} for reaction 15 can be obtained from a plot of the reciprocal half-lives of the peroxy radical decay versus A_0. Figure 5B shows such a plot. The absorbances are corrected for the absorbance due to FO_2. The decay half-lives were derived from a fit to the transient using the second-order expression given in Section 3.3, where $k' = 2k_{15obs}\ \ln 10/(l\sigma_{RO_2}(240\ nm))$. The decays were always well-described by second-order kinetics. For these experiments the optical path length (l) was 80 cm, $[CF_3C(O)OCH_2CF_3]$ = 15 mbar, $[O_2]$ = 15 mbar, $[SF_6]$ = 970 mbar, and the dose was varied between full and 18% of full dose. A linear regression analysis of the data in Figure 5B gives a slope of (2.13 ± 0.06) × 10^5 s^{-1} which can be combined with $\sigma_{240\ nm}(CF_3C(O)OCH(OO\cdot)CF_3)$ = (2.06 ± 0.24) × 10^{-18} cm^2 $molecule^{-1}$ to give k_{15obs} = (7.62 ± 0.91) × 10^{-12} cm^3 $molecule^{-1}$ s^{-1}.

In addition to the self-reaction, the decay of the peroxy radical may also be influenced by reaction with other radicals formed directly or indirectly from the self-reaction, for example HO_2, and $CF_3C(O)OCH(O\cdot)CF_3$:

$$CF_3C(O)OCH(O\cdot)CF_3 + O_2 \rightarrow CF_3C(O)OC(O)CF_3 + HO_2 \quad (19)$$

$$CF_3C(O)OCH(OO\cdot)CF_3 + HO_2 \rightarrow \text{products} \quad (20)$$

$$CF_3C(O)OCH(OO\cdot)CF_3 + CF_3C(O)OCH(O\cdot)CF_3 \rightarrow \text{products} \quad (21)$$

Since the rate constants for reactions 19−21 are unknown, we cannot correct for these reactions at the present time. Our reported value of k_{15obs} is the observed rate constant which describes the rate of decay of absorption at 240 nm in the present system.

3.6. Rate Constant for the Reaction $CF_3C(O)OCH(OO\cdot)CF_3$ + NO → Products. Kinetic data were acquired by monitoring the increase in absorption at 400.5 nm ascribed to NO_2 formation following pulse radiolysis (dose = 22% of maximum) of mixtures containing 15 mbar of $CF_3C(O)OCH_2CF_3$, 15 mbar of O_2, 970 mbar of SF_6, and 0.20−0.81 mbar of NO. The insert in Figure 6 shows a typical experimental trace obtained using a mixture containing 0.61 mbar of NO. For each concentration of NO the increase in absorption was fitted using the following expression: $A(t) = (A_{inf} - A_0)(1 - \exp(-k^{first}t)) + A_0$, where $A(t)$ is the time-dependent absorbance, A_0 is the extrapolated absorbance at $t = 0$ (always close to zero), A_{inf} is the absorbance at infinite time, and k^{first} is the pseudo-first-order appearance rate of NO_2. The smooth line in the insert shows the fit. This technique for measuring the rate constant for the reaction of NO with peroxy radicals is described in detail elsewhere.[14] Figure 6 shows a plot of k^{first} versus the mean NO concentration during the experiment ([NO] − 1/2$[F]_0$). Linear

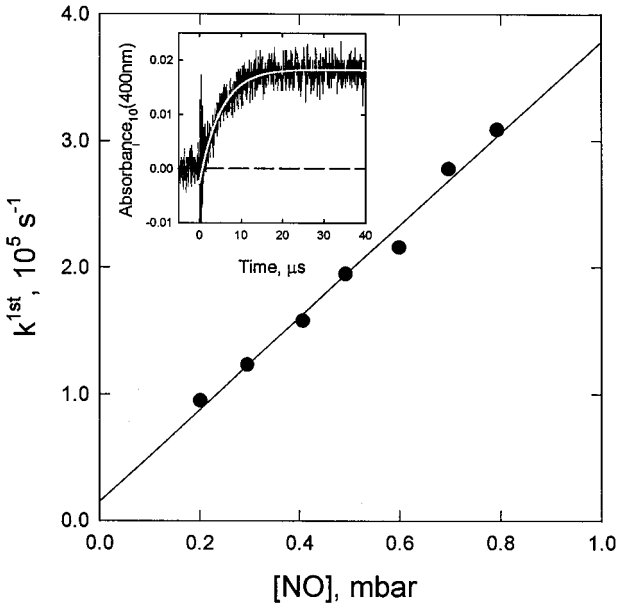

Figure 6. First-order formation rates of NO_2 observed following radiolysis of SF_6/ $CF_3C(O)OCH_2CF_3/O_2/NO$ mixtures as a function of the initial NO concentration. The insert shows a typical experimental trace together with a first-order fit (see text for details).

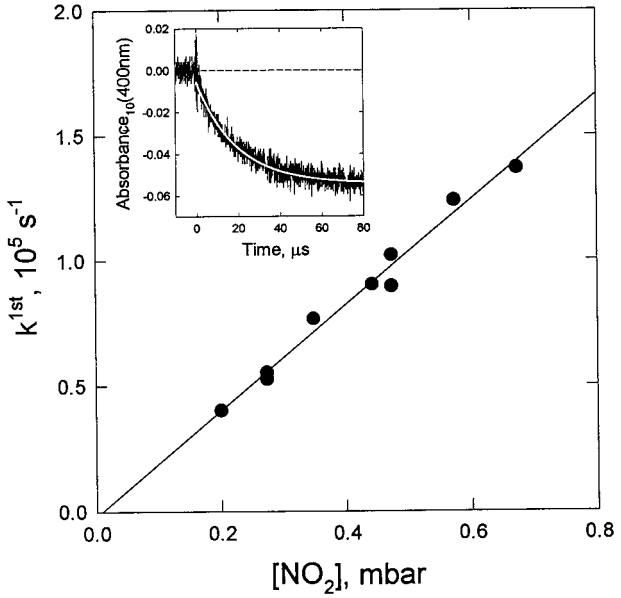

Figure 7. First-order loss rates of NO_2 observed following radiolysis SF_6/ $CF_3C(O)OCH_2CF_3/O_2/NO_2$ mixtures as a function of the initial NO_2 concentration. The insert shows a typical experimental trace together with a first-order fit (see text for details).

least-squares regression of the data in Figure 6 gives $k_3 = (1.5 \pm 0.2) \times 10^{-11}$ cm^3 molecule^{-1} s^{-1}. The NO_2 yield can be calculated from the increase in absorption using $\sigma(NO_2) = 6.0 \times 10^{-19}$ cm^2 molecule^{-1},[15] and when expressed in terms of the initial peroxy radical concentration was 0.87 ± 0.14.

3.7. Rate Constant for the Reaction $CF_3C(O)OCH(OO\cdot)CF_3 + NO_2 + M \rightarrow CF_3C(O)OCH(OONO_2)CF_3 + M$. Kinetic data were acquired by monitoring the decrease in absorption at 400.5 nm ascribed to NO_2 loss following pulse radiolysis (42% of full dose) of mixtures of 15−30 mbar of $CF_3C(O)OCH_2CF_3$, 15−50 mbar of O_2, 920−970 mbar of SF_6, and 0.23−0.70 mbar of NO_2. The insert in Figure 7 shows a typical experimental trace obtained using a mixture containing 0.30 mbar of NO_2. For each concentration of NO_2 the decrease in absorption was fitted using a first-order decay expression. The smooth line in the insert shows the result of such a fit. Figure 7 shows a plot of the resulting pseudo-first-order loss rate constant, k^{first}, versus the mean NO_2 concentration during the experiment, ($[NO_2] - 1/2\times[F]_0$). Linear least-squares analysis of the data in Figure 7 gives $k_4 = (8.5 \pm 0.9) \times 10^{-12}$ cm^3 molecule^{-1} s^{-1}. The value of k_4 obtained here is similar to the high-pressure limiting rate constants for the reactions of other peroxy radicals with NO_2 which lie in the range $(5-10) \times 10^{-12}$ cm^3 molecule^{-1} s^{-1}.[8,9]

3.8. Fate of the $CF_3C(O)OCH(O\cdot)CF_3$ Radical. The fate of the $CF_3C(O)OCH(O\cdot)CF_3$ radical was studied using the UV irradiation of $CF_3C(O)OCH_2CF_3/Cl_2/O_2/N_2$ mixtures in the FTIR−smog chamber system at Ford Motor Company. Experiments were performed at a constant total pressure of 700 Torr with the O_2 partial pressure varied over the range 5−700 Torr. Typical spectra obtained before (A) and after (B) UV irradiation of a mixture containing 4.46 mTorr of $CF_3C(O)OCH_2CF_3$, 0.2 Torr of Cl_2, 37.6 Torr of O_2 at 700 Torr total pressure with N_2 diluent are shown in Figure 8. In all experiments two products $CF_3C(O)OC(O)CF_3$ and $CF_3C(O)OH$ were readily identified and quantified using calibrated reference spectra. The spectral subtraction of $CF_3C(O)OC(O)CF_3$ and $CF_3C(O)OH$ were performed using their characteristic IR features at 1055 and 779 cm^{-1}, respectively. As shown in Figure 9, the increase in $CF_3C(O)OC(O)CF_3$ and $CF_3C(O)OH$ scaled linearly with the loss of $CF_3C(O)OCH_2CF_3$, suggesting that secondary loss or formation processes for these compounds are insignificant.

The reaction of Cl atoms with $CF_3C(O)OCH_2CF_3$ in the presence of O_2 gives rise to peroxy radicals, which in turn will undergo self-reaction to give the corresponding alkoxy radicals:

$$2\ CF_3C(O)OCH(OO\cdot)CF_3 \rightarrow 2\ CF_3C(O)OCH(O\cdot)CF_3 + O_2 \quad (6a)$$

$$2\ CF_3C(O)OCH(OO\cdot)CF_3 \rightarrow CF_3C(O)OC(O)CF_3 + CF_3C(O)OCH(OH)CF_3 + O_2 \quad (6b)$$

There are several possible fates of the $CF_3C(O)OCH(O\cdot)CF_3$ alkoxy radical. Reaction with O_2 gives perfluoro acetic

TABLE 1: Summary of the Kinetic Data Obtained in this Work

reaction	rate constant (cm^3 molecule^{-1} s^{-1})
$F + CF_3C(O)OCH_2CF_3 \rightarrow$ products	$k_{12} = (1.8 \pm 0.2) \times 10^{-12}$
$CF_3C(O)OCH(\cdot)CF_3 + CF_3C(O)OCH(\cdot)CF_3 \rightarrow$ products	$k_{13} = (1.5 \pm 0.2) \times 10^{-11}$
$CF_3C(O)OCH(O_2\cdot)CF_3 + CF_3C(O)OCH(O_2\cdot)CF_3 \rightarrow$ products	$k_{15} = (7.6 \pm 0.9) \times 10^{-12}$
$CF_3C(O)OCH(O_2\cdot)CF_3 + NO \rightarrow$ products	$k_3 = (1.5 \pm 0.2) \times 10^{-11}$
$CF_3C(O)OCH(O_2\cdot)CF_3 + NO_2 \rightarrow$ products	$k_4 = (8.5 \pm 0.9) \times 10^{-12}$
	rate constant ratio[a]
$CF_3C(O)OCH(O\cdot)CF_3 + O_2 \rightarrow CF_3C(O)OC(O)CF_3 + HO_2$	$k_{19}/k_\Delta = (3.6 \pm 0.5) \times 10^{-19}$ cm^3 molecule^{-1}
$CF_3C(O)OCH(O\cdot)CF_3 \rightarrow CF_3C(O)OH + CF_3C(O)\cdot$	$k_{23}/k_\Delta = 0.50 \pm 0.04$

[a] The rate constant ratio is given relative to the total rate constant for decomposition of the alkoxy radical, i.e., $k_\Delta = k_{23} + k_{25} + k_{26}$.

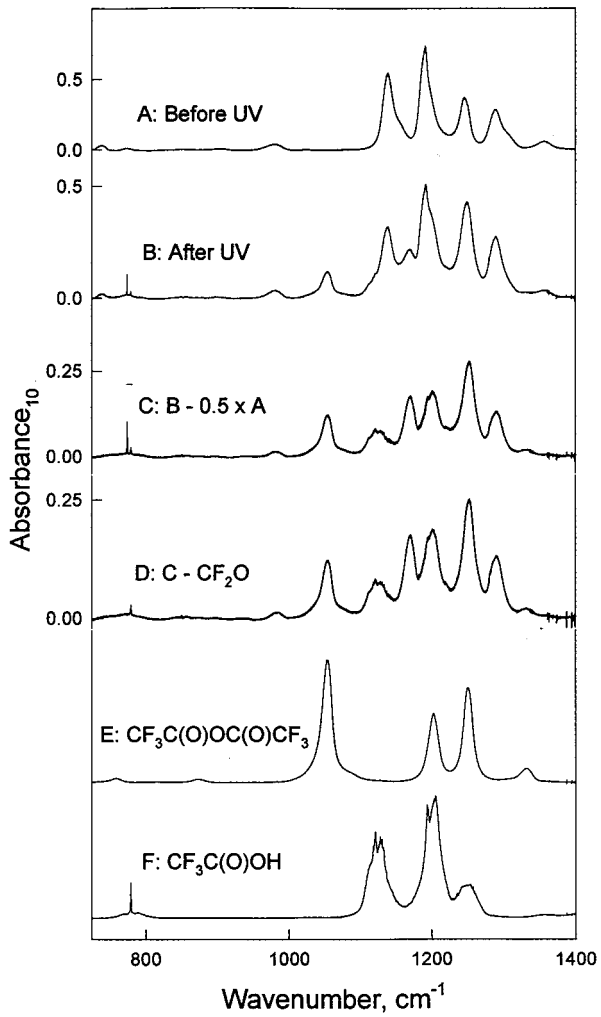

Figure 8. IR spectra acquired before (A) and after (B) a 16 min irradiation of a mixture containing 4.46 mTorr of $CF_3C(O)OCH_2CF_3$, 0.2 Torr of Cl_2, and 37.6 Torr of O_2 in 700 Torr total pressure of N_2 diluent. During the irradiation 50% of $CF_3C(O)OCH_2CF_3$ was consumed. Subtraction of features attributable to $CF_3C(O)OCH_2CF_3$ from panel B gives panel C. Subtraction of features attributable to CF_2O from panel C gives panel D. Panels E and F are reference spectra of $CF_3C(O)OC(O)CF_3$ and $CF_3C(O)OH$.

anhydride, reaction 19. Tuazon et al.[16] have reported that alkoxy radicals of the structure RC(O)OCHO·R′ can undergo α-ester rearrangement to RC(O)OH plus R′C(O)·. In our system α-ester rearrangement will give $CF_3C(O)OH$, reaction 23. The alkoxy radical could also decompose via C−H, C−C, or C−O bond cleavage, reactions 24−26.

$$CF_3C(O)OCH(O\cdot)CF_3 + O_2 \rightarrow CF_3C(O)OC(O)CF_3 + HO_2 \quad (19)$$

$$CF_3C(O)OCH(O\cdot)CF_3 \rightarrow CF_3C(O)OH + CF_3C(O)\cdot \quad (23)$$

$$CF_3C(O)OCH(O\cdot)CF_3 \rightarrow CF_3C(O)OC(O)CF_3 + H \quad (24)$$

$$CF_3C(O)OCH(O\cdot)CF_3 \rightarrow CF_3C(O)OC(O)H + CF_3\cdot \quad (25)$$

$$CF_3C(O)OCH(O\cdot)CF_3 \rightarrow CF_3C(O)O\cdot + CF_3C(O)H \quad (26)$$

Figure 10 shows the observed variation in $CF_3C(O)OC(O)CF_3$ and $CF_3C(O)OH$ yields with oxygen partial pressure. The yield of $CF_3C(O)OC(O)CF_3$ increases while the yield of $CF_3C(O)OH$ decreases with increasing O_2 partial pressure, showing

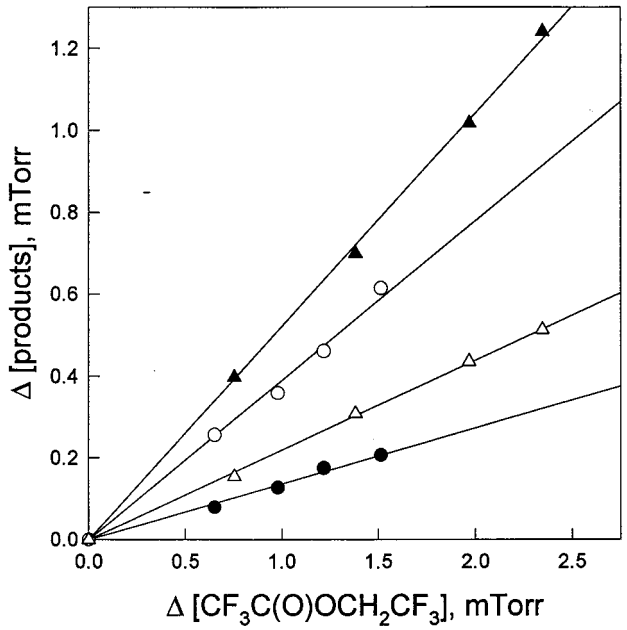

Figure 9. Formation of $CF_3C(O)OC(O)CF_3$ (filled symbols) and $CF_3C(O)OH$ (open symbols) versus loss of $CF_3C(O)OCH_2CF_3$ at a total pressure of 700 Torr in mixtures of 15.5 Torr of O_2, 0.2 Torr of Cl_2, and 3.0 mTorr of $CF_3C(O)OCH_2CF_3$ (circles), and 147 Torr of O_2, 0.3 Torr of Cl_2, and 4.5 mTorr of $CF_3C(O)OCH_2CF_3$ (triangles).

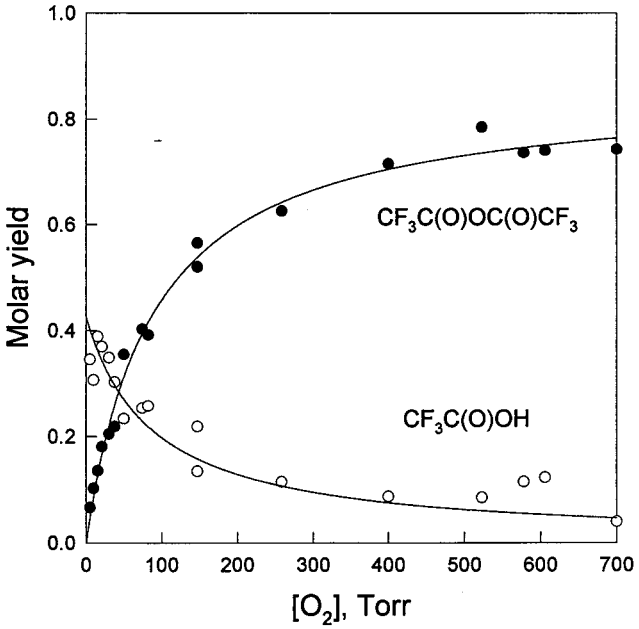

Figure 10. Observed yields of $CF_3C(O)OC(O)CF_3$ (filled symbols) and $CF_3C(O)OH$ (open symbols) versus the O_2 partial pressure following the UV irradiation of $CF_3C(O)OCH_2CF_3/Cl_2/N_2/O_2$ mixtures at 700 Torr total pressure and 296 K. The curves are nonlinear least-squares fit to the data (see text for details).

there is a competition between reactions 19 and 23 for the available $CF_3C(O)OCH(O\cdot)CF_3$ radicals. There is no evidence of a *y*-axis intercept for the $CF_3C(O)OC(O)CF_3$ plot in Figure 10, showing that channels 24 and 6b are unimportant.

After subtraction of the infrared features of $CF_3C(O)OC(O)CF_3$ and $CF_3C(O)OH$, the residual spectra contain features attributable to CF_2O, CF_3OH, $CF_3O_2CF_3$, $CF_3O_3CF_3$, and CO_2. $CF_3O_3CF_3$ and $CF_3O_2CF_3$ were observed only at oxygen concentrations less than 500 Torr. At oxygen concentrations higher than 500 Torr the combined yield of $CF_3C(O)OC(O)CF_3$ and $CF_3C(O)OH$ accounts for ≈85% of the total $CF_3C(O)$-

OCH_2CF_3 loss. At high oxygen concentration only $CF_3C(O)OC(O)CF_3$, $CF_3C(O)OH$, CF_2O, CF_3OH, and CO_2 were observed. When $[O_2] > 500$ Torr the CF_2O yield was less than 10%. The combined yield of $CF_3C(O)OC(O)CF_3$ and $CF_3C(O)OH$ does not account for the total $CF_3C(O)OCH_2CF_3$ loss at low oxygen concentration, suggesting that decomposition of the alkoxy radical via reactions 25 and/or 26 may be significant. $CF_3C(O)OCH_2CF_3$ reacts slowly with Cl atoms ($k = 9.4 \times 10^{-16}$ cm^3 $molecule^{-1}$ s^{-1} [4]). The reactivity of $CF_3C(O)OC(O)H$ toward Cl atoms is unknown, but is expected to be 10−100 times faster than $CF_3C(O)OCH_2CF_3$, on the basis of the rate constants of similar formates (e.g., $k(Cl+CH_3OC(O)OC(O)H) = 1.7 \times 10^{-13}$ cm^3 $molecule^{-1}$ s^{-1} [17] and $k(Cl+CF_3OC(O)H) = 9.8 \times 10^{-15}$ cm^3 $molecule^{-1}$ s^{-1} [7]). Cl atoms react with $CF_3C(O)H$ 4×10^3 times faster than with $CF_3C(O)OCH_2CF_3$.[18] For the $CF_3C(O)OCH_2CF_3$ conversions (10−60%) used in the present study it is expected that any $CF_3C(O)OC(O)H$ and $CF_3C(O)H$ product will be consumed by reaction with Cl atoms.

$$Cl + CF_3C(O)OC(O)H \rightarrow CF_3C(O)OC(O)\cdot + HCl \quad (27)$$

$$Cl + CF_3C(O)H \rightarrow CF_3C(O)\cdot + HCl \quad (28)$$

In the presence of oxygen, $CF_3C(O)\cdot$ radicals are converted into $CF_3C(O)O_2\cdot$, $CF_3C(O)O\cdot$, $CF_3O_2\cdot$, and $CF_3O\cdot$ radicals.[19] The $CF_3C(O)OC(O)\cdot$ radicals are expected to undergo the following reactions:

$$CF_3C(O)OC(O)\cdot + O_2 \rightarrow CF_3C(O)OC(O)O_2\cdot \quad (29)$$

$$CF_3C(O)OC(O)O_2\cdot + RO_2 \rightarrow CF_3C(O)OC(O)O\cdot + RO\cdot + O_2 \quad (30)$$

$$CF_3C(O)OC(O)O\cdot + M \rightarrow CF_3C(O)O\cdot + CO_2 + M \quad (31)$$

$$CF_3C(O)O\cdot + M \rightarrow CF_3\cdot + CO_2 + M \quad (32)$$

Decomposition of $CF_3C(O)OCH(O\cdot)CF_3$ radicals via reactions 25 and 26 will lead to formation of $CF_3C(O)O_x\cdot$ and $CF_3O_x\cdot$ radicals and CO_2. Previous studies in the smog chamber showed that $CF_3O_2CF_3$, $CF_3O_3CF_3$, CF_2O, and CF_3OH are major products in gas mixtures containing $CF_3C(O)O_x\cdot$ and $CF_3O_x\cdot$ radicals.[19] The observed products are consistent with formation of $CF_3C(O)\cdot$ radicals via reaction 23 and also with decomposition of the alkoxy radical via reactions 25 and 26, followed by secondary reactions 27 and 28. Under the present experimental conditions it is not possible to distinguish between channels 25 and 26. Considering that C−O bonds are generally stronger than C−C bonds, decomposition via channel 25 seems more likely than via reaction 26. It has previously been established that the sole fate of $CF_3CH_2OCH(O\cdot)CF_3$ radicals is decomposition to form $CF_3\cdot$ radicals and $CF_3CH_2OC(O)H$.[4] This supports the assumption that C−C bond cleavage is the more favorable channel.

The dependence of the $CF_3C(O)OC(O)CF_3$ and $CF_3C(O)OH$ yields on $[O_2]$ can be expressed in terms of the rate constant ratios k_{19}/k_Δ and k_{23}/k_Δ, where $k_\Delta = k_{23} + k_{25} + k_{26}$. Assuming that the fate of $CF_3C(O)OCH(O\cdot)CF_3$ radicals is reaction with O_2, α-rearrangement, and decomposition via reactions 25 and 26, the yield of $CF_3C(O)OC(O)CF_3$ can be related to the molar yields of the alkoxy radicals and the rate constant ratio k_{19}/k_Δ. The yield of $CF_3C(O)OC(O)CF_3$ is given by

$$Y(CF_3C(O)OC(O)CF_3) = Y(CF_3C(O)OCH(O\cdot)CF_3)\left[\frac{\frac{k_{19}}{k_\Delta}[O_2]}{\frac{k_{19}}{k_\Delta}[O_2]+1}\right] \quad (I)$$

while the yield of $CF_3C(O)OH$ is given by

$$Y(CF_3C(O)OH) = Y(CF_3C(O)OCH(O\cdot)CF_3)\left[\frac{\frac{k_{23}}{k_\Delta}}{\frac{k_{19}}{k_\Delta}[O_2]+1}\right] \quad (II)$$

The yields of $CF_3C(O)OCH(O\cdot)CF_3$ radicals, k_{19}/k_Δ and k_{23}/k_Δ, were derived from nonlinear least-squares fit of eq I and II to the data in Figure 10. The fit to the $CF_3C(O)OH$ data is very sensitive to small $CF_3C(O)OH$ yields from sources other than reaction 23. When reaction mixtures were left to stand in the dark after the end of experiments (50−60% $CF_3C(O)OCH_2CF_3$ consumption) slow formation of $CF_3C(O)OH$ and loss of $CF_3C(O)OC(O)CF_3$ were observed, most likely due to hydrolysis of $CF_3C(O)OC(O)CF_3$. Hydrolysis causes a small underestimation of the $CF_3C(O)OC(O)CF_3$ yield (of the order of 0−2%) and a small overestimation of $CF_3C(O)OH$. At low O_2 concentrations (and low $CF_3C(O)OC(O)CF_3$ yields) hydrolysis is insignificant. Hydrolysis of $CF_3C(O)OC(O)CF_3$ will have little impact on the rate constant ratio derived from the $CF_3C(O)OC(O)CF_3$ data, but will cause a substantial underestimation of k_{19}/k_Δ derived from the $CF_3C(O)OH$ data. The rate constant ratio obtained from the $CF_3C(O)OC(O)CF_3$ data is more reliable. From the $CF_3C(O)OC(O)CF_3$ data we derive $Y(CF_3C(O)OCH(O\cdot)CF_3) = 0.86 \pm 0.04$, and $k_{19}/k_\Delta = 0.0115 \pm 0.0016$ $Torr^{-1}$ ($(3.6 \pm 0.5) \times 10^{-19}$ cm^3 $molecule^{-1}$). Using $Y(CF_3C(O)OCH(O\cdot)CF_3) = 0.86$, and $k_{19}/k_\Delta = 0.0115$ $Torr^{-1}$ in expression (II), we derive $k_{23}/k_\Delta = 0.50 \pm 0.04$ from a one-parameter fit to the $CF_3C(O)OH$ data.

The formation of $CF_3C(O)OH$ observed here confirms the α-ester rearrangement mechanism proposed recently by Tuazon et al.[16] The α-ester rearrangement is expected to involve isomerization through a five-membered transition state of the alkoxy radical. Tuazon et al. showed that α-ester rearrangement is the sole fate of the $CH_3C(O)OCH(O\cdot)CH_3$ radical in air at room temperature and atmospheric pressure. The results presented here show that α-ester rearrangement is a less important channel for the fluorinated analogue, $CF_3C(O)OCH(O\cdot)CF_3$. Using the values of k_{19}/k_Δ, and k_{23}/k_Δ derived above, it can be calculated that in the presence of 1 atm of air ($[O_2] = 160$ Torr), reactions 19 and 23 account for 65 ± 13% and 18 ± 3% of the fate of $CF_3C(O)OCH(O\cdot)CF_3$ radicals, respectively. Presumably, replacement of the electron-donating $-CH_3$ group with the electron-withdrawing $-CF_3$ group reduces the stability of the five-membered ring transition state for the α-ester rearrangement process.

Implications for Atmospheric Chemistry. In the atmosphere, $CF_3C(O)OCH_2CF_3$ will be removed by reaction with OH radicals, photolysis, and/or wet/dry deposition. The atmospheric lifetimes of $CF_3C(O)OCH_2CF_3$ with respect to these processes are unknown at the present, and we cannot estimate their relative importance. We present herein a large body of kinetic and mechanistic data pertaining to the OH radical-initiated oxidation of $CF_3C(O)OCH_2CF_3$ (see Table 1). Reaction

with OH radicals gives the alkyl radical $CF_3C(O)OCH(\cdot)CF_3$. In the atmosphere this alkyl radical will add O_2 to give the corresponding peroxy radical $CF_3C(O)OCH(OO\cdot)CF_3$. We show here that the peroxy radical reacts rapidly with NO to produce NO_2 and, by inference, $CF_3C(O)OCH(O\cdot)CF_3$ radicals. Using $k_3 = 1.5 \times 10^{-11}$ cm^3 molecule^{-1} s^{-1} together with an estimated background tropospheric NO concentration of 2.5×10^8 molecule cm^{-3}, the lifetime of the peroxy radicals with respect to reaction with NO is calculated to be 4 min. We show here that there are three loss processes of the $CF_3C(O)OCH(O\cdot)CF_3$ radicals. In one atmosphere of air at 296 K, 65% of the $CF_3C(O)OCH(O\cdot)CF_3$ radicals will react with O_2 to form $CF_3C(O)OC(O)CF_3$, 18% will undergo α-ester rearrangement to form $CF_3C(O)OH$ and $CF_3C(O)\cdot$ radicals, while the fate of the remaining 17% is unclear at this time.

Acknowledgment. We thank Andrei Guschin for help in performing the FTIR experiments, Steve Japar for helpful comments, and the Commission of the European Communities for financial support of the work at Risø.

References and Notes

(1) Molina, M. J.; Rowland, F. S. *Nature* **1974**, *249*, 810.

(2) Farman, J. D.; Gardiner, B. G.; Shanklin, J. D. *Nature* **1985**, *315*, 207.

(3) Product information sheet from 3M Specialty Chemicals Division, 1996.

(4) Wallington, T. J.; Gushin, A.; Stein, T. N. N.; Platz, J.; Sehested, J.; Christensen, L. K.; Nielsen, O. J. *J. Phys. Chem. A* **1998**, *102*, 1152.

(5) Wallington, T. J.; Scheider, W. F.; Sehested, J.; Bilde, M.; Platz, J.; Nielsen, O. J.; Christensen, L. K.; Molina, M. J.; Molina, L. T.; Wooldrige, P. W. *J. Phys. Chem. A* **1997**, *101*, 8264.

(6) Christensen, L. K.; Sehested, J.; Nielsen, O. J.; Bilde, M.; Wallington, T. J.; Gushin, A.; Molina, M. J.; Molina, L. T. *J. Phys. Chem. A* **1998**, *102*, 4839.

(7) Christensen, L. K.; Wallington, T. J.; Gushin, A.; Hurley, M. D. *J. Phys. Chem. A.* **1999**, *103*, 4202.

(8) Wallington, T. J.; Dagaut, P.; Kurylo, M. *J. Chem. Rev.* **1992**, *92*, 667.

(9) Lightfoot, P. D.; Cox, R. A.; Crowley, J. N.; Destriau, M.; Hayman, G. D.; Jenkin, M. E.; Moortgat, G. K.; Zabel, F. *Atmos. Environ*. **1992**, *26A*, 1805.

(10) Hansen, K. B.; Wilbrandt, R.; Pagsberg, P. *Rev. Sci. Instr*. **1979**, *50*, 1532.

(11) Wallington, T. J.; Japar, S. M. *J. Atmos. Chem*. **1989**, *9*, 399.

(12) Ellermann, T.; Sehested, J.; Nielsen, O. J.; Pagsberg, P.; Wallington, T. *Chem. Phys. Lett*. **1994**, *218*, 287.

(13) Maricq, M. M.; Szente, J. J. *J. Phys. Chem.* **1992**, *96*, 4925.

(14) Sehested, J.; Nielsen, O. J.; Wallington, T. J. *Chem. Phys. Lett*. **1993**, *213*, 457.

(15) DeMore, W. B.; Sander, S. P.; Golden, D. M.; Hampson, R. F.; Kurylo, M. J.; Howard, C. J.; Ravishankara, A. R.; Kolb, C. E.; Molina, M. J. *Jet* Propulsion Laboratory Publication 1997, 97-4.

(16) Tuazon, E. C.; Aschmann, S. M.; Atkinson, R.; Carter, W. P. L. *J. Phys. Chem. A* **1998**, *102*, 2316.

(17) Bilde, M.; Møgelberg, T. E.; Sehested, J.; Nielsen, O. J.; Wallington, T. J.; Hurley, M. D.; Japar, S. M.; Dill, M.; Orkin, V. L.; Buckley, T. J.; Huie, R. E.; Kurylo, M. *J. Phys. Chem. A* **1997**, *101*, 3514.

(18) Wallington, T. J.; Hurley, M. D. *Int. J. Chem. Kinet.* **1993**, *25*, 819.

(19) Wallington, T. J.; Hurley, M. D.; Nielsen, O. J.; Sehested J. *J. Phys. Chem.* **1994**, *98*, 5686.